GSURE criterion for unsupervised regularized reconstruction in tomographic diffractive microscopy

L. Denneulin, F. Momey, D. Brault, M. Debailleul, A M Taddese, N. Verrier, O. Haeberlé

GSURE criterion for unsupervised regularized reconstruction in Tomographic Diffractive Microscopy

L. Denneulin[1,*], F. Momey[1], D. Brault[1], M. Debailleul[2], A. M. Taddese[2], N. Verrier[2], and O. Haeberlé[2]

[1] Laboratoire Hubert Curien UMR CNRS 5516, Université Jean Monnet, F-42000 Saint-Étienne, France
[2] Institut Recherche en Informatique, Mathématiques, Automatique et Signal (IRIMAS UR UHA 7499), Université de Haute-Alsace, IUT Mulhouse, 61 Rue Albert Camus, 68093 Mulhouse Cedex, France
[*] Corresponding author: laurence.denneulin@univ-st-etienne.fr

Compiled December 17, 2021

We propose an unsupervised regularized inversion method for the reconstruction of the 3D refractive index map of a sample in Tomographic Diffractive Microscopy (TDM). It is based on the minimization of the Generalized Stein's Unbiased Risk Estimator (GSURE) to automatically estimate optimal values for the hyperparameters of one or several regularization terms (sparsity, edge-preserving smoothness, Total Variation). We evaluate the performance of our approach on simulated and experimental limited-view data. Our results show that GSURE is an efficient criterion to find suitable regularization weights, that is a critical task, particularly in the context of reducing the amount of required data to allow faster yet efficient acquisitions and reconstructions.

http://dx.doi.org/10.1364/ao.XX.XXXXXX

1. INTRODUCTION

Optical microscopy techniques constitute the reference tools for the study of biological phenomena, thanks to their capability of imaging living specimens. Among them, three dimensional (3D) imaging techniques are of great interest because they allow the observed specimens to keep their natural 3D structure and properties. In this context, advanced fluorescence nanoscopy methods (STED [1], PALM/STORM [2–4]) are able to achieve high resolved 3D images above ten times beyond the diffraction limit. However, they require long acquisition times which can be incompatible with live imaging. Moreover, the required labelling of the sample is a complex and invasive technique that can degrade the specimen. In this case, label-free imaging techniques are preferred but must be adapted to observe transparent samples. Optical diffraction tomography (ODT) or Tomographic Diffractive Microscopy (TDM) is an emergent technique, which permits to image transparent specimens in 3D [5], without preparation or staining. TDM brings a morphological information about the observed objects. It is less specific and less resolved than fluorescence-based nanoscopy techniques which focus on precise metabolic targets (kernels, mitochondria, etc.). However, this information is complementary as it can allow to register anatomical (TDM) and functional (fluorescence) phenomenons. Moreover, TDM allows for the imaging of a wider field-of-view at a resolution up to twice larger than the diffraction limit, and possibly at a very fast acquisition range. It is almost similar to Structured Illumination Microscopy (SIM) that also performs a kind of synthesis aperture of the object's spectral content, and can go further than twice the diffraction limit.

TDM is an interferometric imaging technique based on digital holographic measurements in tomographic mode, *i.e.* for multiple illuminations and/or sample orientations. Thus, acquisitions are performed by either a specimen rotation or an illumination scanning (one projection orientation per hologram). It gives access, by image reconstruction, to the 3D refractive index (RI) map of a specimen.

Several reconstruction methods from TDM measurements have been proposed in the last decades. The first Born or Rytov approximation allows for a direct 3D mapping of the object in the Fourier space, combining each view's 2D Fourier spectrum. Thus, an isotropic exploration of the object, for example by combination of illumination orientations and sample rotations, leads to a fully-3D mapping of the object's spectrum and allows to reach an isotropic resolution in the 100nm range [6, 7]. However, this reconstruction quality requires a huge number of holograms with almost isotropic exploration. Moreover, the Born or Rytov inversion is limited to weakly scattering samples. To overcome limitations involved in classical inversion, one has to turn to more sophisticated approaches. The Gerchberg-Papoulis algorithm [8] proposes an iterative framework based on the alternating projections principle - similar to the so-called Fienup Error Reduction algorithm in 2D digital holography [9] - with the imposition of a positivity (or negativity) constraint on the RI difference map. This algorithm is a representative of what we call inverse problems approaches [8, 10, 11]. These last are mostly based on the minimization of a global penalty criterion constructed as a combination of two components: a so-called data-fidelity term measuring the error between the data and an image formation model, and one or several priors taking the form of regularization terms or bound constraints. Inverse approaches are more flexible because they allow for the use of more accurate models, *e.g.* multiple-scattering based approaches

[12–15]. Thanks to this gain of accuracy, the data information is better exploited. Therefore, the useful amount of measurements can be drastically reduced if an appropriate trade-off is found between the relative influences given on both the data-fidelity and the *a priori* information on the targeted object. This trade-off is most of the time achieved by weighting properly the regularization penalty terms in the global criterion. These scalar weights are called hyperparameters, and their tuning is critical to ensure the consistency of the inverse problem and thus its solution.

The optimal hand tuning of the hyperparameters is a too fastidious task, so finding unsupervised tuning approaches is of great interest in image reconstruction. If the ground truth was known, the optimal hyperparameters' values would be those that minimize an error between the reconstruction and the ground truth (e.g. the estimation Mean Square Error). Obviously in practice, such a ground truth being unknown, unsupervised tuning approaches consist in using a "blind" criterion to find optimal values for the hyperparameters. Popular methods in this context are the generalized cross-validation (GCV:[16]), the *L*-curve [17], hierarchical Bayesian strategies [18] and the Generalized Stein unbiased Risk Estimator (GSURE: [19, 20]). Lately, some hyperparameters-free methods have exploited neural networks for learning appropriate regularizers [21, 22].

In this work, we discuss the performance of GSURE for the unsupervised tuning of the regularization hyperparameters in the context of TDM reconstruction. The application of GSURE in such a context constitutes the main contribution of this work. Our paper is organized as follows. In Section 2 we introduce the TDM principle with some mathematical notations, and present the forward model used in our experiments. In Section 3, we present a regularized inverse approach for TDM reconstruction that involves popular regularization terms (sparsity, edge-preserving, Total Variation), which we "plug" in a minimization procedure of the GSURE criterion to estimate optimal regularization hyperparameters. Finally, in Section 4, we evaluate the performance of our unsupervised reconstruction approach using GSURE, on both simulated and real data. Our datasets consist in realistic simulations of TDM acquisitions of a single transparent bead (5 and 10 µm diameter), using a Lorenz-Mie scattering model [23], and experimental TDM acquisitions of a Jerusalem artichoke pollen grain (∼ 30 µm diameter). We perform the reconstructions from very limited TDM views to show how the optimal trade-off between the data-fidelity and the regularization is helpful in this context. Our results tend to demonstrate this claim.

2. TDM DATA ACQUISITION PRINCIPLE AND FORWARD MODEL

A. Object and data models

We consider a single object (e.g. a bead as in Fig. 1), or a distribution of objects, immersed in a medium of RI n_0. In the following, the object in the medium is sampled and considered as the three dimensional (3D) array $\mathbf{n} \in \mathbb{C}^K$, where K is the total number of voxels. Each voxel value $\mathbf{n}_k$, for $k \in \{1, \cdots, K\}$, is the complex RI difference of the object with the medium in this voxel. Hence each $\mathbf{n}_k$ can be decomposed into two components $\mathfrak{Re}(\mathbf{n}_k)$ and $\mathfrak{Im}(\mathbf{n}_k)$, defining its respective real and imaginary parts such that $\mathbf{n}_k = \mathfrak{Re}(\mathbf{n}_k) + j\mathfrak{Im}(\mathbf{n}_k)$. Moreover, $\mathbf{n}_k = 0$ means that the voxel $k \in \{1, \cdots, K\}$ contains only the medium.

A TDM dataset consists in the recording, on a digital sensor of M pixels, of L complex holograms obtained by the diffraction and propagation into the sample of L respective coherent illumination plane waves $\underline{u}_\ell^{(inc)}$ that are tilted with respect to the sensor plane (see Fig. 1). We denote $\mathbf{d}_{\ell *} \in \mathbb{C}^M$ the ℓ^{th} sampled complex hologram corresponding to a unique tilted view of parameter ϕ_ℓ.

The model of the respective noisy data acquired by the camera is given as:

$$\mathbf{d}_\ell = \mathbf{d}_\ell^* + \boldsymbol{\eta}_\ell \quad \textbf{(1)}$$

where $\boldsymbol{\eta}_\ell$ corresponds to a vector of M noise values.

B. The hologram formation model

In practice, the true complex holograms $\mathbf{d}_{\ell *} \in \mathbb{C}^M$ are unknown. Several methods exist [14] to calculate an approximation of these projections as the first Born or Rytov approximation [5, 24–26], the beam propagation method (BPM) and similar strategies such the wave propagation method (WPM) [10, 27], the Lippmann-Schwinger model [28], etc. We denote by $u_\ell(\mathbf{n})$ the hologram formation model. In this work, we focus on BPM that performs a cascading propagation of the diffracted wave through the sample - from the "top" to the "bottom" - decomposed in several slices, each one interacting successively with the upper wave (multiplication of the wave with the transmittance slice). This model is adapted to simulate multiple scattering (in the propagation direction) into a dense volume. However, the unsupervised method proposed in this paper can be applied using another hologram formation model. The forward-model, approximating the true data formation process, is thus the following:

$$\mathbf{d}_\ell \approx u_\ell(\mathbf{n}) + \boldsymbol{\eta}_\ell \quad \textbf{(2)}$$

Note that this model is now an approximation of the true data formation process in Eq. (1) because of the additional modeling errors.

3. PROPOSED METHOD

A. Regularized inverse approach

We aim at retrieving $\mathbf{n} \in \mathbb{C}^K$ from the complex dataset $(\mathbf{d}_\ell)_{\ell \in \{1,\ldots,L\}}$. The classical inverse approach is to find $\mathbf{n}$ mini-

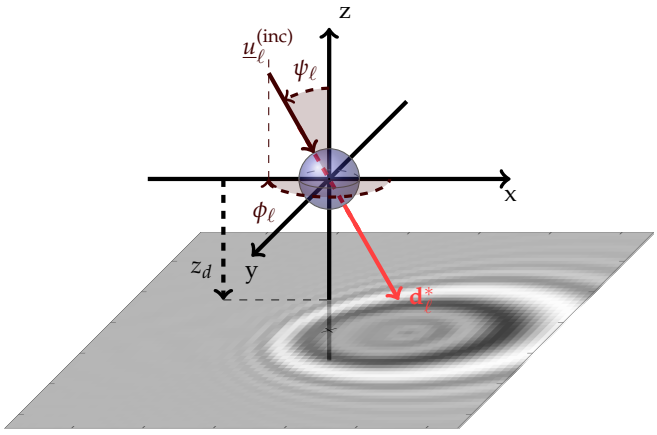

Fig. 1. Scheme of the TDM principle for the ℓ-th hologram acquisition $\mathbf{d}_\ell^*$ of a sample (here a bead). The hologram is acquired for an orientation of illumination wave $\underline{u}_\ell^{(inc)}$, parametrized by the angles ψ_ℓ in the (z, x) plane and ϕ_ℓ in the (x, y) plane, at a distance z_d from the center of the object.

mizing the following cost function:

$$f(\mathbf{n}) = \sum_{\ell=1}^{L} \frac{1}{2} \left\| \mathbf{d}_\ell - u_\ell(\mathbf{n}) \right\|_{\mathbb{C}}^2. \tag{3}$$

It is equivalent to the co-log-likelihood minimization under the assumption that $\forall \ell \in \{1, \dots, L\}$, $\mathbf{d}_\ell \sim \mathcal{N}(u_\ell(\mathbf{n}), \sigma^2 \mathbf{Id}_M)$ (*i.e.* the additive noise $\boldsymbol{\eta}_\ell$ follows a centered multidimensional Gaussian distribution of diagonal covariance $\sigma^2 \mathbf{Id}_M$) . However, the minimization of the problem Eq. 3 alone can lead to strong artifacts in the reconstruction if the problem is ill-posed: a good conditionment of the problem is critical to control and alleviate modeling errors and noise amplification in the reconstruction process.

To palliate this issue, a prior term $g^{\boldsymbol{\rho}}$ is added to the problem Eq. 3, that can be a composition of one or several regularizers, and parametrized by a set of hyperparameters $\boldsymbol{\rho}$. This set is composed of at least one hyperparameter per regularization term to weight their contribution. The reconstruction problem of the 3D RI map $\mathbf{n}$ becomes:

$$\widehat{\mathbf{n}} \in \underset{\mathbf{n} \in \Omega}{\arg\min} \left\{ f(\mathbf{n}) + g^{\boldsymbol{\rho}}(\mathbf{n}) \right\} \tag{4}$$

where $\Omega \subset \mathbb{C}^K$ is a set of separable bound constraints applied on the real and imaginary part of each element of $\mathbf{n}$.

In this work we compare two regularizations: $g^{\text{EP}+\ell_1}$ that is the combination of an Edge Preserving smoothing prior [29] and the ℓ_1-norm sparsity constraint (EP + ℓ_1) applied separately on the real part $\mathfrak{Re}(\mathbf{n})$ and imaginary part $\mathfrak{Im}(\mathbf{n})$ of $\mathbf{n}$, and g^{TV} the Total Variation (TV) [30]. On one hand, the EP+ℓ_1 regularization, given by:

$$\begin{aligned} g^{\text{EP}+\ell_1}(\mathbf{n}) = \lambda^{\text{EP}} \sum_{n=1}^{N} \left(\sqrt{\|\mathbf{D}_n \mathbf{n}\|^2 + \mu^2} - \mu \right) \\ + \lambda^{\ell_1} \sum_{n=1}^{N} \left(|\mathfrak{Re}(\mathbf{n}_n)| + |\mathfrak{Im}(\mathbf{n}_n)| \right) \end{aligned} \tag{5}$$

has the advantage of being differential (thanks to the relaxing parameter $\mu > 0$) when all the voxels of $\mathbf{n}$ are constrained to have the same sign. $\mathbf{D}_n$ is a finite difference operator at each voxel n, giving a vector of six components: three gradient components for both the real part $\mathfrak{Re}(\mathbf{n})$ and imaginary part $\mathfrak{Im}(\mathbf{n})$ of $\mathbf{n}$. Thus the squared norm $\|\mathbf{D}_n \mathbf{n}\|^2$ applied to this gradient vector is the sum of its six squared components. When μ tends to zero, the Edge Preserving Smoothing tends to TV. The ℓ_1 sparsity prior applied on $\mathbf{n}$ is there to ensure zero values outside of the object, thus it acts as a support constraint. In such a case of regularization, the set of hyperparameters is $\boldsymbol{\rho} = (\lambda^{\text{EP}}, \mu, \lambda^{\ell_1})$. The whole criterion in Eq. 4 is differentiable (smooth), so we achieve the minimization using the VMLM-B algorithm [31], which is a limited memory quasi-newton method with line search.

On the other hand, the Total Variation, given by:

$$g^{\text{TV}}(\mathbf{n}) = \lambda^{\text{TV}} \sum_{n=1}^{N} \sqrt{\|\mathbf{D}_n \mathbf{n}\|^2}. \tag{6}$$

requires only one hyperparameter, thus $\boldsymbol{\rho} = \lambda^{\text{TV}}$. This regularization is not differentiable and the criterion in Eq. 4 is then a sum of a smooth (f) and a non-smooth (g^{TV}) terms. This leads to the use of proximal algorithms for the minimization of the cost function. In this work, we use the primal-dual Condat-Vũ algorithm with backtracking [32–34].

B. GSURE for unsupervised reconstruction

An appropriate tuning of the regularization hyperparameters is essential to achieve a good reconstruction of the object. An under-regularized reconstruction will lead to a wrong estimation of the 3D map $\mathbf{n}$. For example, the "missing cone" effect, a classical problem in TDM due to the limited angular coverage, will be exhibited by the defective closure of the object in the axial (z) direction. On the contrary, an over-regularized reconstruction can yield over-smoothing, i.e. a loss of details. The tuning of the hyperparameters can be achieved by finding the set $\boldsymbol{\rho}$ for which the reconstruction optimizes a given quality criterion, for example: the estimation Mean Square Error (MSE), the absolute error, or the prediction Mean Square Error (pMSE). These three quality criterions require the knowledge of the ground truth, unknown in practice, but the pMSE can be estimated using the Generalized Stein's Unbiased Risk Estimator [19, 20] which requires only the knowledge of the data $\mathbf{d}_\ell$.

We denote $\widehat{\mathbf{n}}_{\boldsymbol{\rho}}$ the reconstruction obtained for a given set of hyperparameters $\boldsymbol{\rho}$. The pMSE is defined as follows:

$$\text{pMSE}(\widehat{\mathbf{n}}_{\boldsymbol{\rho}}) = \sum_{\ell=1}^{L} \mathbb{E}\left[\|\mathbf{d}_\ell^* - u_\ell(\widehat{\mathbf{n}}_{\boldsymbol{\rho}})\|_{\mathbb{C}}^2 \right]. \tag{7}$$

where $\mathbb{E}$ stands for the expectation. Note that the use of such a criterion to find $\boldsymbol{\rho}$ for which the reconstructions is minimizing the pMSE requires an accurate image formation model. In fact, this criterion only "sees" the data and the modeling approximations. If it is not accurate enough, the pMSE minimization will lead to a reconstruction minimizing these modeling errors at the expense of its accordance to the ground truth object.

The GSURE criterion is given by:

$$\text{GSURE}(\widehat{\mathbf{n}}_{\boldsymbol{\rho}}) = \sum_{\ell=1}^{L} \left[\frac{1}{2\sigma^2} \left\| \mathbf{d}_\ell - u_\ell(\widehat{\mathbf{n}}_{\boldsymbol{\rho}}) \right\|_{\mathbb{C}}^2 + 2\text{tr}\left(\frac{\partial u_\ell(\widehat{\mathbf{n}}_{\boldsymbol{\rho}})}{\partial \mathbf{d}_\ell} \right) - M \right]. \tag{8}$$

where σ^2 is the variance of the noise in the data, tr stands for the trace (sum of the diagonal elements) of a matrix, and M the number of pixel in each hologram. Since GSURE is an estimator of the pMSE, then

$$\mathbb{E}[\text{GSURE}(\widehat{\mathbf{n}}_{\boldsymbol{\rho}})] = \text{pMSE}(\widehat{\mathbf{n}}_{\boldsymbol{\rho}}) \tag{9}$$

and both criterion, as a function of $\boldsymbol{\rho}$, achieve their minimum for the same argument.Hence, we can find the optimal hyperparameter set $\hat{\boldsymbol{\rho}}$ minimizing the pMSE, by minimizing GSURE.

The trace term $\text{tr}(\partial u_\ell(\widehat{\mathbf{n}}_{\boldsymbol{\rho}})/\partial \mathbf{d}_\ell)$ is equal to $\text{div}\, u_\ell(\widehat{\mathbf{n}}_{\boldsymbol{\rho}})$ and is obtained with the Monte-Carlo method presented in [35]. Its principle is to generate a perturbed dataset $\mathbf{d}_\ell^\delta$ by adding a random deviation on the data $(\mathbf{d}_\ell)_{\ell \in \{1,\dots,L\}}$, with a centered Gaussian noise of standard deviation ε. Then a reconstruction from $\mathbf{d}_\ell^\delta$ is performed to obtain a map $\widehat{\mathbf{n}}_{\boldsymbol{\rho}}^\delta$. From this reconstruction, the computation of the trace is performed from the following formula:

$$\text{tr}\left(\frac{\partial u_\ell(\widehat{\mathbf{n}}_{\boldsymbol{\rho}})}{\partial \mathbf{d}_\ell} \right) = \frac{\left\langle \mathbf{d}_\ell^\delta - \mathbf{d}_\ell, u_\ell(\widehat{\mathbf{n}}_{\boldsymbol{\rho}}^\delta) - u_\ell(\widehat{\mathbf{n}}_{\boldsymbol{\rho}}) \right\rangle}{\varepsilon^2}. \tag{10}$$

A good choice of ε is critical to ensure GSURE is a good estimate of the pMSE. If chosen too small or too large, the trace will be underestimated or overestimated, leading to a wrong GSURE criterion. In this work we compute ε as the tenth of the median of the real part of the data, which gives a good GSURE criterion in practice.

To achieve the minimization of GSURE, the most intuitive method is to create a mapping of different hyperparameters set $\boldsymbol{\rho}$, to proceed to the reconstruction on both datasets and perturbed datasets to compute GSURE for each $\boldsymbol{\rho}$, and finally find on the mapping the set $\widehat{\boldsymbol{\rho}}$ that gives the minimum of the obtained discretized GSURE map. However, such a method can become computationally intractable when the set $\boldsymbol{\rho}$ is composed with two or more hyperparameters. Hence, an optimization of the GSURE criterion is performed using a Powell method [36], which does not require the computation of the gradient for the search of the minimum.

4. RESULTS

In this section, we observe and discuss the performance of our GSURE based unsupervised method on reconstructions from simulated and experimental data.

First, we consider simulated TDM measurements of a perfect sphere of diameter Δ, using the realistic Lorenz-Mie scattering model [23], that simulates the diffracted field from this kind of object almost perfectly. For the reconstruction, we choose the BPM model that fits at best the simulated one and overcomes the classical Born or Rytov model, particularly when the size of the object of interest or the RI gradient grows. Moreover, the simplicity of the object of interest (a homogeneous sphere with sharp edges) corresponds exactly to the chosen Edge-Preserving and TV regularizers (promoting piecewise constant images) as its characteristics validate precisely such prior assumptions. Hence, our choices lead to a really good toy model and an "inverse crime"-less reconstruction, allowing the validation of our method. We aim to prove that we can find optimal values of the hyperparameters in the sense of the prediction Mean Square Error (pMSE), under such controlled conditions.

Second, we consider experimental TDM acquisitions of a Jerusalem artichoke pollen grain. We aim to validate the conclusion obtained on simulated data.

A. Results on a simulated bead

We aim at reconstructing independently three non-centered spherical beads of different diameters Δ (see Table. 1), with a RI $n_{bead} = 1.45$ and immersed in a medium of RI $n_0 = 1.519$ - mimicking a silica bead in immersion oil. For each bead, our datasets consist in L on-focus holograms $\mathbf{d}_\ell^*$ (i.e. $z_d = 0\,\mu$m), simulated from an implementation of the Lorenz-Mie model [23]. The incident wave orientations are displayed on Fig. 2 and the size of the holograms are given in Table. 1. Finally, we compute the data following Eq. 1, where each element $\boldsymbol{\eta}_k$ of the additive noise vector $\boldsymbol{\eta}$ is randomly generated using a stationary complex normal law $\mathcal{CN}(0, 2\sigma^2)$ with $\sigma^2 = 0.1$. Table. 1 summa-

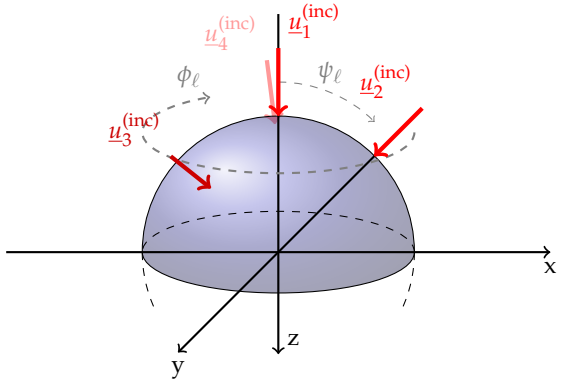

Fig. 2. Scheme of the L projections parametrized by the angles $\psi_\ell \in \{0°, 45°, 45°, 45°\}$ and $\phi_\ell \in \{0°, 0°, 120°, 240°\}$.

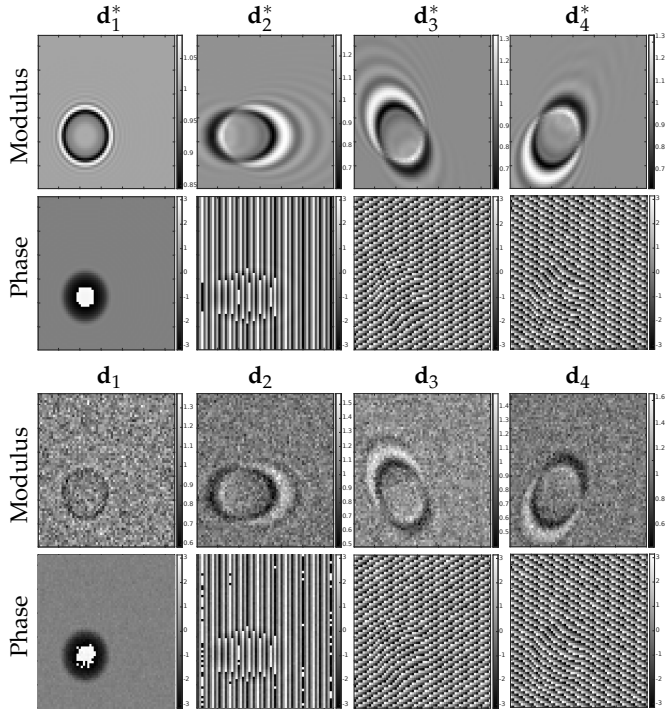

(a) $\Delta = 5\mu$m

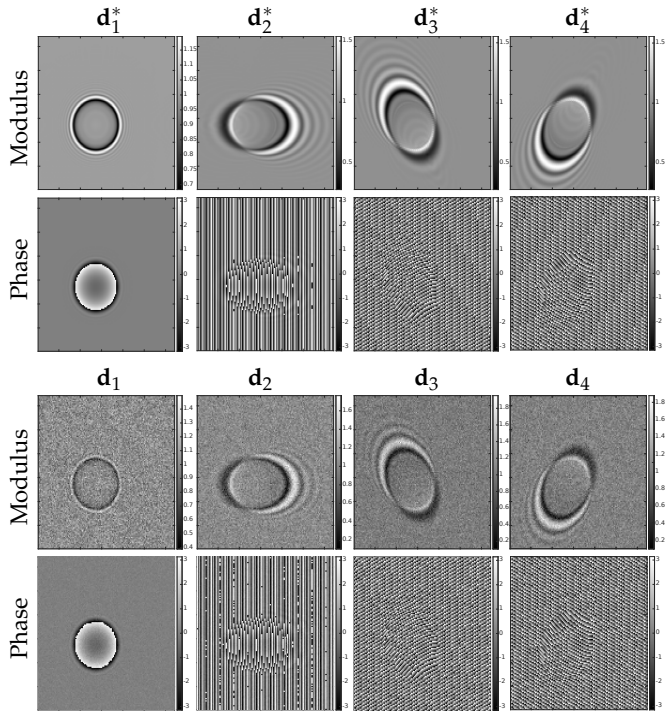

(b) $\Delta = 10\mu$m

Fig. 3. Moduli and phases of the true holograms $\mathbf{d}_\ell^*$ and of the related data $\mathbf{d}_\ell$, for $\ell \in \{1, \ldots, 4\}$, simulated with the Lorenz-Mie model for the parameters summarized in Table. 1.

Table 1. Summary of the beads and data properties, and list of the regularization hyperparameters obtained with the Powell minimization of the GSURE criterion.

case	Δ	$(x_{\text{bead}}, y_{\text{bead}}, z_{\text{bead}})$	ψ_L	L	M	N	$\rho^{\text{EP}+\ell_1}$	ρ^{TV}
(a)	5μm	$(-2.3467\mu\text{m}, -2.3467\mu\text{m}, 0\mu)$	45°	4	64×64	$64 \times 64 \times 64$	$(10^{0.38}, 10^{-0.27}, 10^{-0.99})$	$10^{-0.67}$
(b)	10μm	$(-2.3467\mu\text{m}, -2.3467\mu\text{m}, 0\mu)$	45°	4	128×128	$128 \times 128 \times 128$	$(10^{1.53}, 10^{0.44}, 10^{-1.4})$	$10^{0.49}$

rizes the simulations parameters. The modulus and the phase of the Lorenze-Mie simulations for all the incidences are displayed on Fig. 3 along with the modulus and the phase of the data.

Since the difference between the Lorenze-Mie model and BPM is growing with the RI difference and with the size, the case (a) in Table 1 is an intermediate case and the case (b) is the harder case. We only consider $L = 4$ projections. More projections could make the task easier but we make the choice to show configurations where the tuning of regularizations is critical to get the best trade-off with the accordance to the data model.

Fig. 4 presents the maps (respectively curves), of pMSE values and GSURE, for the EP+ℓ_1 regularization (respectively TV). First of all, we can see that the minimal arguments on both criteria, are close. In the case of EP+ℓ_1, the μ hyperparameter is fixed to the best hyperparameter obtained with the Powell method. For this regularization GSURE seems to be less sensitive to the ℓ_1 norm, which can be problematic since the sparsity constraint is important to have a good support of the object, *i.e.* to have zero values outside of the object.

Fig. 5 shows the 3D reconstructions of the bead compared to the ground truth in the different configurations. For each case and each regularization, the bead is well reconstructed. The reconstructions with the EP + ℓ_1 regularization seems noisier than with the TV regularization and the edges of the object are smoother. Such an observation is coherent with the assertion that for EP + ℓ_1 the GSURE criterion is less sensitive to the ℓ_1 norm. In fact, since the reconstruction is under-regularized for the sparsity-promoting part, the values outside the support of the object are not sufficiently constrained to zero. Moreover, it leads to a smoothing of the edges along the z-axis. On the opposite, the edges in the reconstructions with TV are sharp, and the medium is uniform and noiseless. The reconstruction with TV is thus satisfying and seems really close to the ground

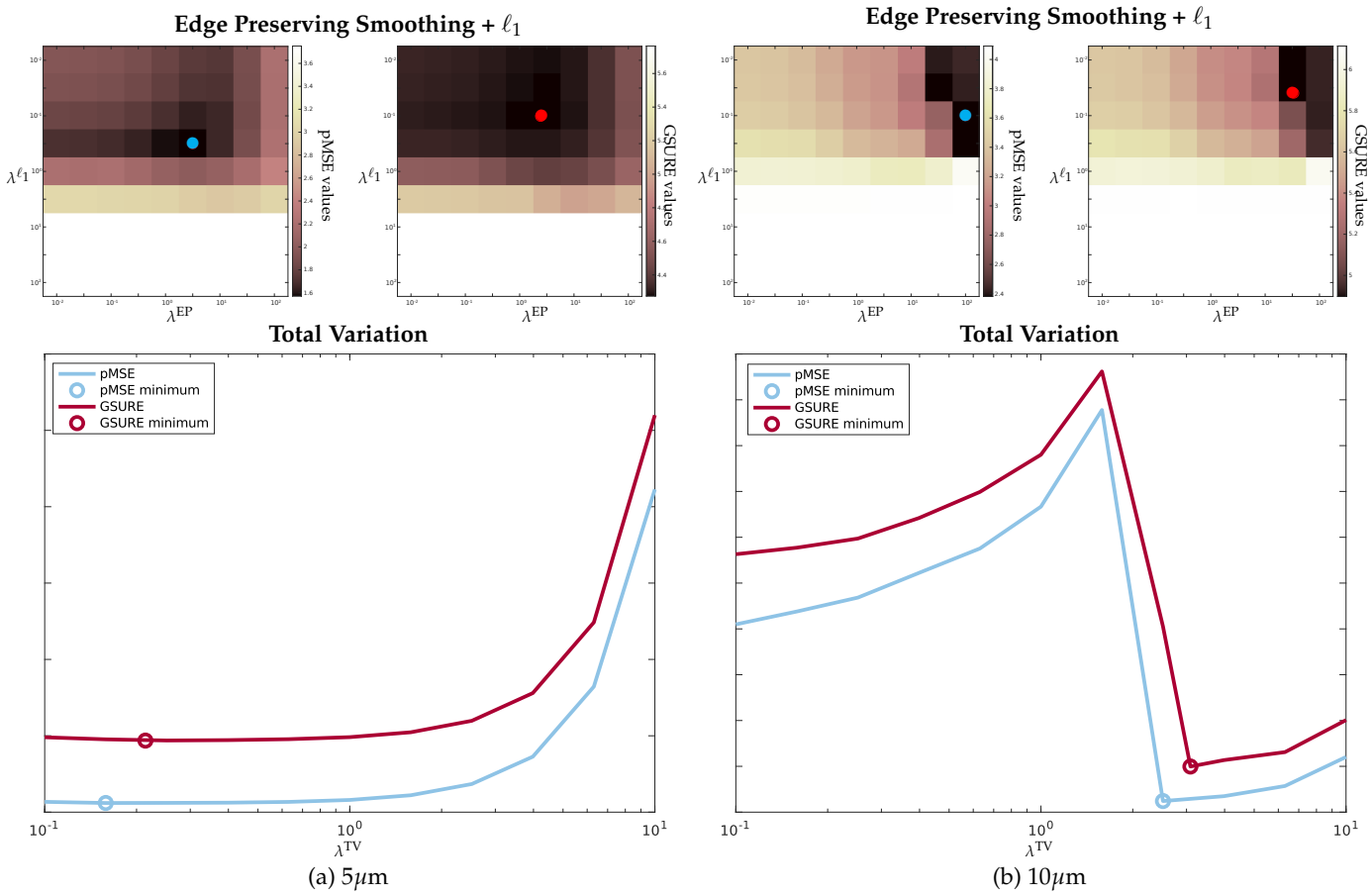

Fig. 4. Maps of pMSE and GSURE values for both regularizations and for each case presented in Table 1. For EP+ℓ_1, the values of μ are fixed to those estimated (see Table. 1). The minimum of the pMSE (respectively GSURE) values are marked with a blue (respectively red) circle.

truths.

An overview of under-regularized and over-regularized reconstructions, in the case of the TV regularization, is presented in Fig. 6. For the under-regularized case, the object is not well defined. The edges and the inner region are lost. This highlights the fact that the amount of data, in this simulation configuration and with such hyperparameters, is not sufficient to reconstruct the bead correctly, evidencing the need of appropriately tuned regularizations. For the over-regularized case, the bead is well defined but some artifacts are appearing.

Overall, the GSURE criterion seems to be an effective tool to select automatically a good set of hyperparameters for the reconstruction as it manages to capture a set of optimal regularization weights ensuring a satisfactory solution that fits at best the data model and the prior constraint.

To compare which regularization term, for the best set of hyperparameters estimated by GSURE, gives the best performances, we perform a quantitative study of the RI difference distribution in the reconstructed bead in Fig.7. In case (a) and (b), the median with EP+ℓ_1 is closer to the true RI than with TV. However, the interquartile range is smaller with TV than with EP+ℓ_1. In the end, with EP+ℓ_1, since the bead is less compact

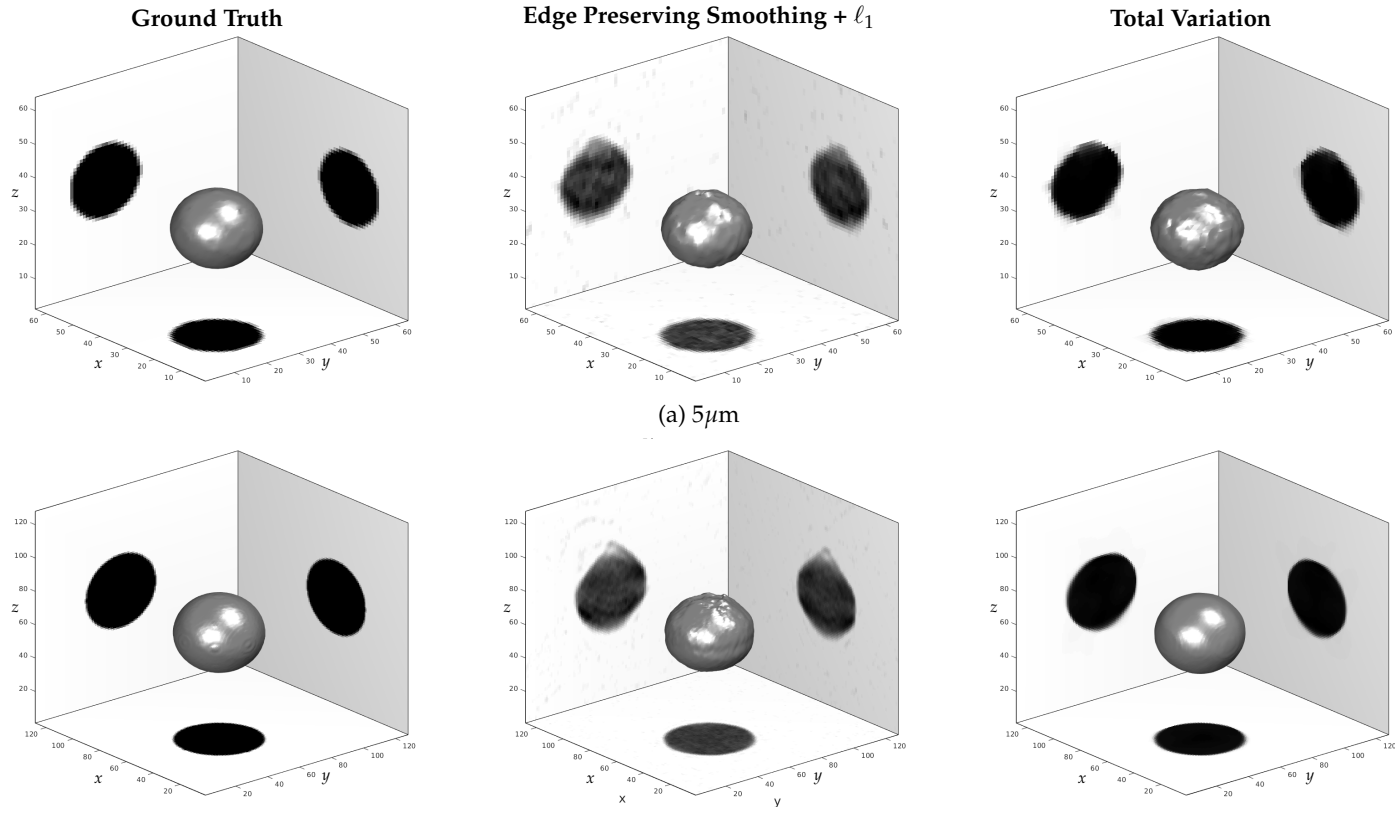

Fig. 5. 3D segmented views of the ground truth and reconstructed beads obtained with optimal regularization weights minimizing GSURE, for both regularization terms EP + ℓ_1 and TV, and each case presented in Table 1. Side views displays the xy, xz and yz orthogonal slices through the object's center.

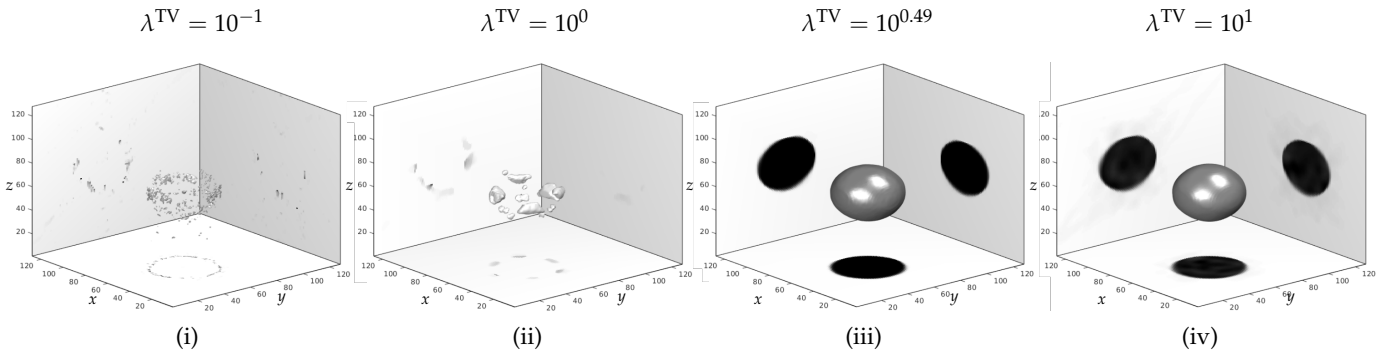

Fig. 6. Reconstructions of the bead (b) with the TV regularization for several choices of hyperparameters and with the optimal parameter obtained with the minimization of the GSURE criterion. Case (i) and (ii) are under-regularized reconstructions, case (iii) is the reconstruction minimizing the GSURE criterion and case (iv) is over-regularized.

due to an under-regularization, the precision on the RI difference is worse than with TV. Yet, with TV, the average RI difference obtained in the bead is smaller than the ground truth. Note that a loss of intensity is common with TV.

To conclude, in these simulations GSURE is effective to tune automatically the hyperparameters leading to reconstruction with a satisfying quality, a difficult task due to the low amount of data in this context. The reconstruction with TV gives better results than with EP+ℓ_1 because GSURE is less sensitive to the sparsity-promoting constraint. However, it suffers from a bias in the reconstructed RI difference in the bead. Note that this object has a piecewise constant gradient, thus the TV regularization is at ease in this context. With a more detailed object such a prior can be too strong and lead to the flattening of some structures. This is why in the following we still apply both regularizers.

B. Results on a pollen grain sample

We used the GSURE criterion to reconstruct the 3D index map of a Jerusalem artichoke pollen grain. These data are given with the courtesy of the IRIMAS laboratory, Mulhouse, France. A detailed description of the TDM setup that performed the measurements can be found in [7]. It is based on holographic measurements in off-axis configuration. In our reconstructions, the considered dataset is the measured complex diffracted waves on the sensor plane (focal plane of the setup), extracted from the raw off-axis measurements.

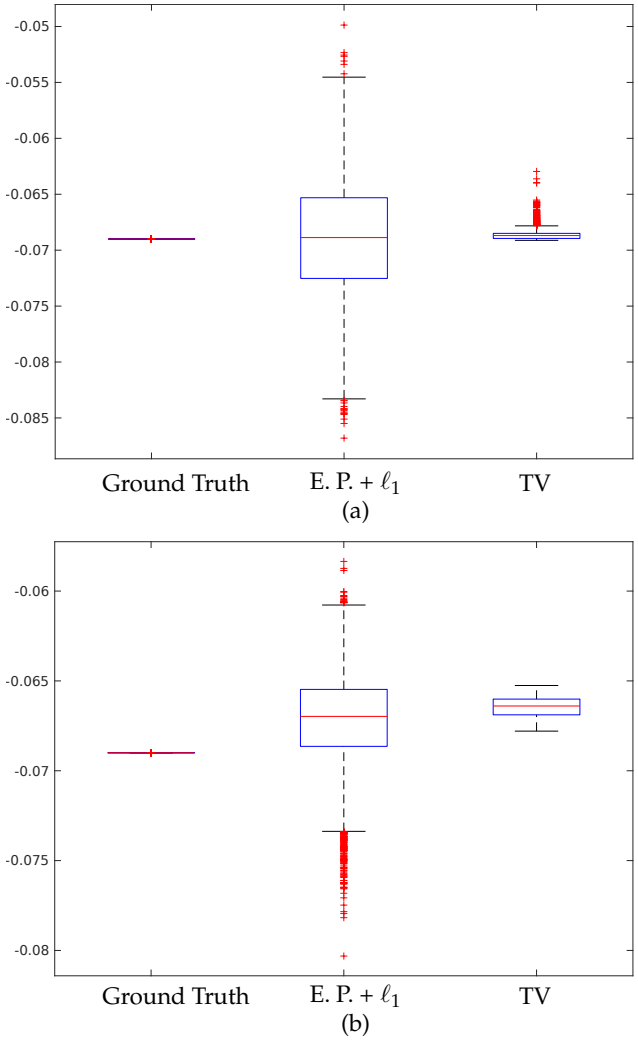

Fig. 7. Distribution of the RI difference value of the reconstructed beads giving the best GSURE for both regularization and each case presented in Table 1. Each blue boxes corresponds to the interquartile range and the red line is the median. The red crosses represent the outliers.

To estimate the noise in the data, we suppose it is an homogeneous Gaussian noise and estimate its variance on a patch containing only background. We proceed to the GSURE optimization for the reconstruction with EP+ℓ_1 and TV regularizations respectively, using only $L = 20$ projections. These projections are chosen by the following method. First we sort the entire set of 600 projections by their angles ϕ_ℓ and group them in 20 subsets. Thus, we ensure that the 20 subsets are covering the entire circle on which ϕ_ℓ evolves. Then, one projection is randomly chosen in each subset to create the dataset. Since problem Eq.4 is non-convex due to the BPM approximation, to avoid the convergence to a local minimum [12], we initiate the reconstruction obtained with an unregularized inversion using the first Born approximation [5, 24–26]. We made the hypothesis that the object has no absorption (*i.e* $\mathfrak{Im}(\mathbf{n}_k) = 0$ for all $k \in \{1, \dots, N\}$) and that the object's absolute RI values are larger than the medium RI value n_0 (the RI difference is greater or equal to 0), leading to the following separable bound constraints set:

$$\Omega = \left\{ \mathbf{n} \in \mathbb{R}^N \mid \forall k \in \{1, \dots, N\},\ \mathbf{n}_k \geq 0 \right\}. \tag{11}$$

Figure 8 presents different views of the object reconstructed with a direct inversion using Rytov approximation for $L = 600$ without any constraint or regularization (courtesy from IRIMAS team), with the Gerchberg-Papoulis (GP [8]) method including a non-negativity constraint for $L = 600$ and $L = 20$, and with the presented method for both regularization terms. The set of hyperparameters obtained for the reconstructions are $\boldsymbol{\rho}^{\text{EP}+\ell_1} = (10^{0.61}, 10^{-3.53}, 10^{0.84})$ and $\boldsymbol{\rho}^{\text{TV}} = 10^{-0.26}$. First, comparing Rytov and GP reconstructions for $L = 600$, we see that the constraint on the sign of the RI difference improves clearly the contrast and, as in [8], alleviate the underestimation of RI values. Thus, the reconstruction with GP seems better, and this is why we consider it as our "ground truth" for our comparisons with $L = 20$.

For both reconstructions using our method, the object is well reconstructed and the contrast is enhanced compared with GP for $L = 20$. On the TV reconstruction, even if the apparent resolution is lower than for the Rytov and GP reconstructions (for $L = 600$), we can observe the same structured features inside the object. For example, in Fig. 8: (a)-(c) and (e), we highlighted some dense regions with red arrows and kind of porosities with purple arrows. These features are better reconstructed with our methods than with GP for $L = 20$. However, the reconstruction with EP+ℓ_1 is a little smoother than the reconstruction with TV, leading to the loss of these small features. Finally, our methods deal better with the zero values outside the object (support estimation). It is mainly visible in the 3D views in rows (e) and (g) and for the central frame (*i.e.* $z = 256$) shown on row (b). Furthermore, we can see on row (f) that our methods deal also better with the missing cone effect.

Fig. 9 presents wrongly tuned reconstructions of the pollen grain with the TV regularization. We can see that in the under-regularized case, the contrast is slightly lighter, and some porosities are lost in case (a) and (b). However, the reconstruction is close to the reconstruction obtained with GSURE even though

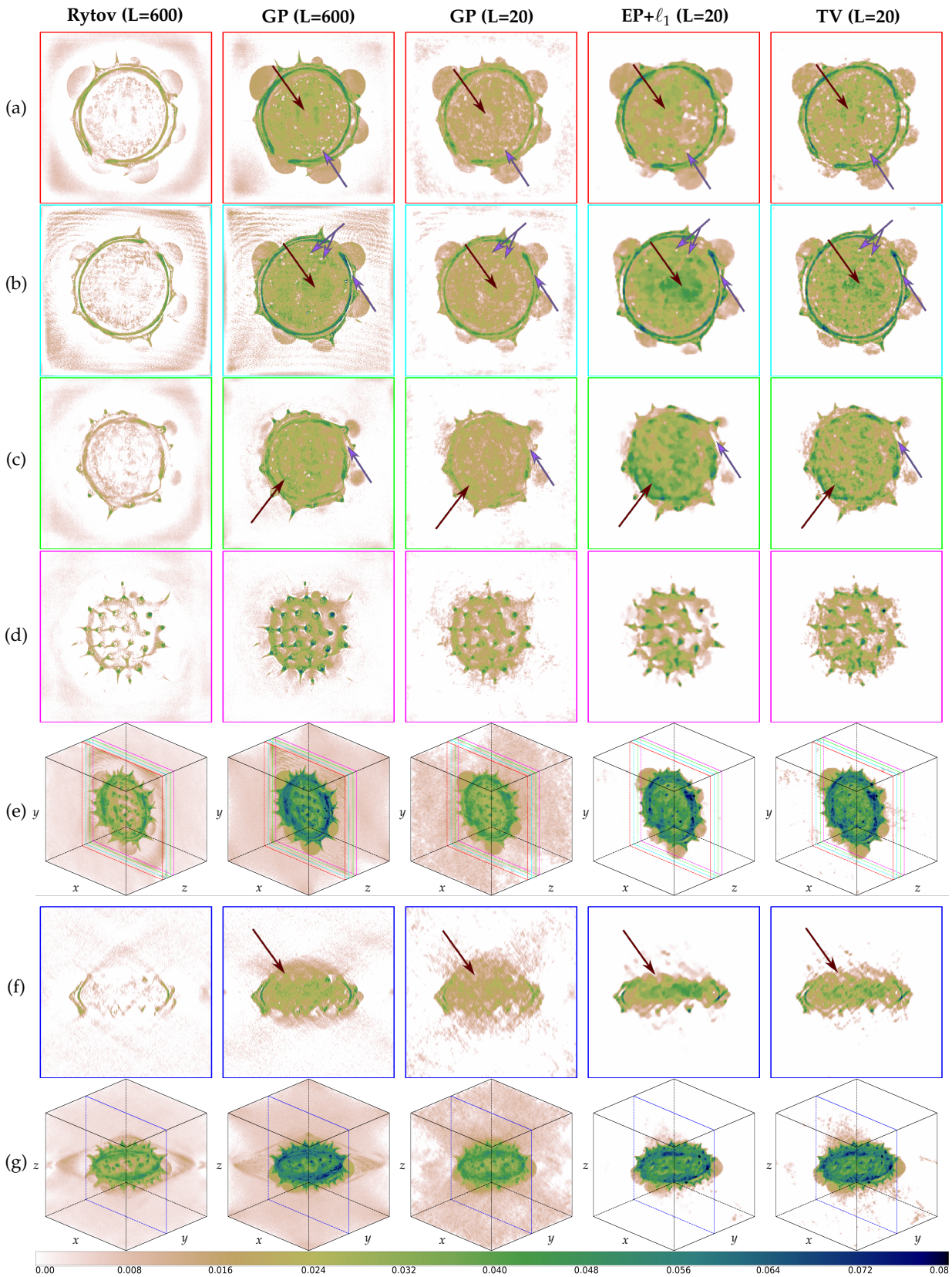

Fig. 8. Views of the Jerusalem artichoke pollen grain for the Rytov inversion and with the GP method for $L = 600$ projections, and the reconstructions with the GP method and giving the best GSURE values for the EP+ℓ_1 and TV regularizations for $L = 20$ projections. Rows (a)-(d) represents the (x, y) slices for $z \in \{231, 256, 282, 303\}$ and are highlighted on the (x, y, z) 3D view on row (e) with the same colored frames. Row (f) is the (x, z) view for $y = 256$ and is highlighted on the (x, z, y) 3D view on row (g) with the same colored frame.

the hyperparameter is a lot smaller. In the over-regularized case, all the details are lost. The reconstruction is really different from the reconstruction obtained with GSURE even though the hyperparameter is not far from the optimal one (in the sense of the pMSE).

In conclusion, in this experimental case, when using the TV regularization, the optimization of the GSURE criterion is effective to achieve a satisfying reconstruction. In the case of EP+ℓ_1, some further hand tuning could help lower the regularization and recover the features inside the object. Thus, it only gives a starting set. Overall, an important point in these experiments is the demonstration that an appropriate tuning of the regularization hyperparameters can favor a better exploitation of the data by the model, opening the way to drastically reduce the amount of useful TDM projections (from an order of magnitude in this experiment) while preserving a satisfying reconstruction in terms of contrast and resolution.

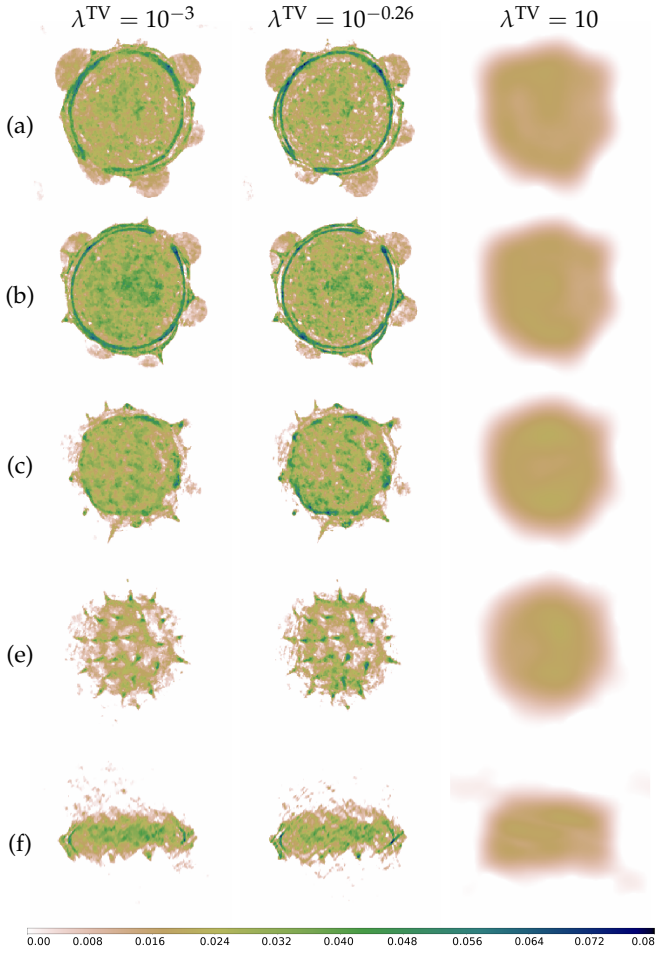

Fig. 9. Comparison of reconstructions of the pollen grain, on the slices Fig.8-(a) to (c), (e), and (f), with the TV regularization for different hyperparameters. From the left to the right : an under-regularized reconstruction, the reconstruction giving the best GSSURE value and an over-regularized reconstruction.

5. CONCLUSION

In this work, we propose an unsupervised method for automatically tune the hyperparameters of a regularized 3D reconstruction method from TDM measurements using GSURE. We applied it with both differentiable and non-differentiable regularization terms. We prove its capability to find a good tuning of the regularization hyperparameters on both simulated and experimental data. This work show how an appropriate tuning of the hyperparameters helps to exploit at best the data information, which is particularly critical when the amount of measurements is or has to be reduced, for example for experiment or setup optimization purposes.

However, this work only presents a brief application of GSURE and raises several perspectives. First, it would be interesting to study how GSURE behaves with other models (*e.g.* the first Born Approximation). Second, an empirical study of how the GSURE minimal argument varies with the number of projections used for the reconstruction could be useful to see if it is predictable. Such a case would allow us to tune the hyperparameters only on a few holograms (the minimum required) and then perform a reconstruction with all the data (or a sufficient amount to have the best quality). Third, an optimization of the computational time could be done. In fact, it takes two reconstructions to compute one iteration of GSURE and several iterations are needed to converge to its minimum. Depending on the complexity of the hologram formation model (Born or BPM), it can take several hours to several days. Finally, a comparison with other autotunning method should be performed.

6. ACKNOWLEDGEMENTS

The pollen grain data used in this work are given with the courtesy of the IRIMAS laboratory, Mulhouse, France.

7. FUNDING

This work is funded by the ANR **HORUS** (ANR-18-CE45-0010) : **H***igh* **O***ptical* **R***esolution for* **U***nlabeled* **S***amples*.

8. DISCLOSURES

The authors declare no conflict of interest.

9. DATA AVAILABILITY

Data underlying the results presented in this paper are not publicly available at this time but may be obtained from the authors upon reasonable request.

REFERENCES

1. T. A. Klar, S. Jakobs, M. Dyba, A. Egner, and S. W. Hell, "Fluorescence microscopy with diffraction resolution barrier broken by stimulated emission," Proc. Natl. Acad. Sci. **97**, 8206–8210 (2000).
2. E. Betzig, G. H. Patterson, R. Sougrat, O. W. Lindwasser, S. Olenych, J. S. Bonifacino, M. W. Davidson, J. Lippincott-Schwartz, and H. F. Hess, "Imaging intracellular fluorescent proteins at nanometer resolution," Science **313**, 1642–1645 (2006).
3. M. J. Rust, M. Bates, and X. Zhuang, "Sub-diffraction-limit imaging by stochastic optical reconstruction microscopy (storm)," Nat. methods **3**, 793–796 (2006).
4. S. T. Hess, T. P. Girirajan, and M. D. Mason, "Ultra-high resolution imaging by fluorescence photoactivation localization microscopy," Biophys. journal **91**, 4258–4272 (2006).

5. O. Haeberlé, K. Belkebir, H. Giovaninni, and A. Sentenac, "Tomographic diffractive microscopy: basics, techniques and perspectives," J. Mod. Opt. **57**, 686–699 (2010).
6. M. Debailleul, B. Simon, V. Georges, O. Haeberlé, and V. Lauer, "Holographic microscopy and diffractive microtomography of transparent samples," Meas. Sci. Technol. **19**, 074009 (2008).
7. B. Simon, M. Debailleul, M. Houkal, C. Ecoffet, J. Bailleul, J. Lambert, A. Spangenberg, H. Liu, O. Soppera, and O. Haeberlé, "Tomographic diffractive microscopy with isotropic resolution," Optica **4**, 460–463 (2017).
8. J. Lim, K. Lee, K. H. Jin, S. Shin, S. Lee, Y. Park, and J. C. Ye, "Comparative study of iterative reconstruction algorithms for missing cone problems in optical diffraction tomography," Opt. Express **23**, 16933–16948 (2015).
9. J. R. Fienup, "Phase retrieval algorithms: a comparison," Appl. Opt. **21**, 2758–2769 (1982).
10. U. S. Kamilov, I. N. Papadopoulos, M. H. Shoreh, A. Goy, C. Vonesch, M. Unser, and D. Psaltis, "Learning approach to optical tomography," Optica **2**, 517–522 (2015).
11. A. Berdeu, F. Momey, B. Laperrousaz, T. Bordy, X. Gidrol, J.-M. Dinten, N. Picollet-D'hahan, and C. Allier, "Comparative study of fully three-dimensional reconstruction algorithms for lens-free microscopy," Appl. Opt. **56**, 3939–3951 (2017).
12. U. S. Kamilov, I. N. Papadopoulos, M. H. Shoreh, A. Goy, C. Vonesch, M. Unser, and D. Psaltis, "Optical Tomographic Image Reconstruction Based on Beam Propagation and Sparse Regularization," IEEE Transactions on Comput. Imaging **2**, 59–70 (2016).
13. H. Y. Liu, U. S. Kamilov, D. Liu, H. Mansour, and P. T. Boufounos, "Compressive imaging with iterative forward models," in *2017 IEEE International Conference on Acoustics, Speech and Signal Processing (ICASSP),* (2017), pp. 6025–6029.
14. R. Eckert, N. Repina, M. Chen, Y. Liang, R. Ng, and L. Waller, "Modeling Light Propagation in 3d Phase Objects," in *Imaging and Applied Optics 2017 (3D, AIO, COSI, IS, MATH, pcAOP) (2017), paper DW2F.2,* (Optical Society of America, 2017), p. DW2F.2.
15. T.-A. Pham, E. Soubies, A. Goy, J. Lim, F. Soulez, D. Psaltis, and M. Unser, "Versatile reconstruction framework for diffraction tomography with intensity measurements and multiple scattering," Opt. Express **26**, 2749–2763 (2018).
16. G. H. Golub, M. Heath, and G. Wahba, "Generalized cross-validation as a method for choosing a good ridge parameter," Technometrics **21**, 215–223 (1979).
17. P. C. Hansen and D. P. O'Leary, "The use of the l-curve in the regularization of discrete ill-posed problems," SISC **14**, 1487–1503 (1993).
18. R. Molina, "On the hierarchical bayesian approach to image restoration: applications to astronomical images," IEEE Transactions on Pattern Analysis Mach. Intell. **16**, 1122–1128 (1994).
19. C. M. Stein, "Estimation of the mean of a multivariate normal distribution," The annals Stat. pp. 1135–1151 (1981).
20. Y. C. Eldar, "Generalized sure for exponential families: Applications to regularization," IEEE Transactions on Signal Process. **57**, 471–481 (2008).
21. F. Yang, F. Yang, T.-a. Pham, H. Gupta, M. Unser, and J. Ma, "Deep-learning projector for optical diffraction tomography," Opt. Express **28**, 3905–3921 (2020). Publisher: Optical Society of America.
22. K. C. Zhou and R. Horstmeyer, "Diffraction tomography with a deep image prior," Opt. express **28**, 12872–12896 (2020).
23. F. Slimani, G. Grehan, G. Gouesbet, and D. Allano, "Near-field lorenz-mie theory and its application to microholography," Appl. Opt. **23**, 4140–4148 (1984).
24. E. Wolf, "Three-dimensional structure determination of semi-transparent objects from holographic data," Opt. Commun. **1**, 153–156 (1969).
25. A. J. Devaney, "Inverse-scattering theory within the Rytov approximation," Opt. Lett. **6**, 374 (1981).
26. Y. Sung, W. Choi, C. Fang-Yen, K. Badizadegan, R. R. Dasari, and M. S. Feld, "Optical diffraction tomography for high resolution live cell imaging," Opt. Express **17**, 266 (2009).
27. X. Ma, W. Xiao, and F. Pan, "Optical tomographic reconstruction based on multi-slice wave propagation method," Opt. express **25**, 22595–22607 (2017).
28. T.-a. Pham, E. Soubies, A. Ayoub, J. Lim, D. Psaltis, and M. Unser, "Three-Dimensional Optical Diffraction Tomography With Lippmann-Schwinger Model," IEEE Transactions on Comput. Imaging **6**, 727–738 (2020). Conference Name: IEEE Transactions on Computational Imaging.
29. P. Charbonnier, L. Blanc-Féraud, G. Aubert, and M. Barlaud, "Deterministic edge-preserving regularization in computed imaging," IEEE TIP **6**, 298–311 (1997).
30. L. I. Rudin, S. Osher, and E. Fatemi, "Nonlinear total variation based noise removal algorithms," Phys. D: Nonlinear Phenom. **60**, 259–268 (1992).
31. E. Thiébaut, "Optimization issues in blind deconvolution algorithms," in *Astronomical Data Analysis II,* vol. 4847 (International Society for Optics and Photonics, 2002), pp. 174–183.
32. L. Condat, "A Primal–Dual Splitting Method for Convex Optimization Involving Lipschitzian, Proximable and Linear Composite Terms," J. Optim. Theory Appl. **158**, 460–479 (2013).
33. B. C. Vũ, "A Splitting Algorithm for Coupled System of Primal–Dual Monotone Inclusions," J. Optim. Theory Appl. **164**, 993–1025 (2015).
34. L. Denneulin, N. Pustelnik, M. Langlois, I. Loris, and É. Thiébaut, "Primal-dual splitting scheme with backtracking for handling with epigraphic constraint and sparse analysis regularization," (iTwist, Nantes, France, Dec. 2-4, 2020., 2020).
35. S. Ramani, T. Blu, and M. Unser, "Monte-Carlo Sure: A Black-Box Optimization of Regularization Parameters for General Denoising Algorithms," IEEE TIP **17**, 1540–1554 (2008).
36. M. J. Powell, "The newuoa software for unconstrained optimization without derivatives," in *Large-scale nonlinear optimization,* (Springer, 2006), pp. 255–297.